

ORIGINAL ARTICLE

Computed Tomography and Magnetic Resonance Anatomy of the Normal Orbit and Eye of the Horse

C. D'Août¹, J. F. Nisolle², M. Navez², R. Perrin³, T. Launois³, L. Brogniez³, P. Clegg⁴, F. Hontoir¹ and J. M. Vandeweerd^{1*}

Addresses of authors: ¹ Department of Veterinary Medicine, Integrated Veterinary Research Unit-Namur Research Institute for Life Sciences (IRVU-NARILIS), University of Namur, Namur, Belgium;

² Centre Hospitalier Universitaire (CHU) de Mont Godinne, Université Catholique de Louvain, Yvoir, Belgium;

³ Clinique Desbrosse, Saint Lambert des Bois, France;

⁴ Department of Musculoskeletal Biology, Faculty of Health and Life Sciences, University of Liverpool, Neston, UK

***Correspondence:**

Tel.: +32495703728;

fax: +3281724376;

e-mail: jean-michel.vandeweerd@fundp.ac.be

With 11 figures

Received July 2014; accepted for publication August 2014

doi: 10.1111/ah.12149

Summary

Traumatic and infectious diseases of the eye and orbit can occur in horses. For diagnosis and monitoring of such diseases, medical imaging is useful including computed tomography (CT) and magnetic resonance imaging (MRI). The aim of the current study was to describe CT and MRI anatomy of the equine orbit and ocular globe. The heads from four adult horses were scanned with a 6-slice Emotion 6 CT (Siemens, Erlangen), and a 3.0 Tesla Siemens Verio 6 MRI using T1 and T2-weighted sequences. To validate CT and MR reference images, these were compared with anatomical models and gross anatomical sections. The bony limits of the orbital cavity, the relationship of the orbit with sinuses and foramina of the skull were well identified by CT. MRI was useful to observe soft tissues and was able to identify adnexae of the ocular globe (eyelids, periorbital fat, extraocular muscles, lacrymal and tarsal glands). Although MRI was able to identify all components of the eye (including the posterior chamber), it could not differentiate sclera from choroid and retina. The only nerve identified was the optic nerve. Vessels were not seen in this series of cadaver heads. This study showed that CT and MRI are useful techniques to image the equine orbit and eye that can have clinical applications.

Introduction

The horse has a prominent eye and orbit which is prone to both traumatic and infectious diseases (Schaer, 2007). For the diagnosis and monitoring of such diseases, medical imaging is sometimes necessary (Ramirez and Tucker, 2004). Ultrasonography (US) is a rapid, safe and practical method that is commonly used to investigate the ocular globe (Williams and Wilkie, 1996; Penninck et al., 2001; Bentley et al., 2003). Conversely, radiography is of limited help as it does not identify soft tissues accurately and osseous structures are often superimposed (Caha et al., 1994). Computed tomography (CT) and magnetic resonance (MR) can provide cross-sectional and three-dimensional images of the eye so that the spatial relationship between anatomical structures can be assessed (Dennis,

2000; Penninck et al., 2001). CT and MRI are now common in referral centres, as well as in numerous equine and small animal practices in the UK, USA and Europe. However, there is few peer-reviewed information about CT and MRI ocular anatomy.

A CT anatomy study of the cranium, brain, paranasal sinuses, nasal cavity and teeth has been conducted in the horse, but anatomy relating to the orbit was not specifically described (Morrow et al., 2000). In another CT study of two foals, only a limited number of structures were identified (zygomatic arch, zygomatic process of frontal bone, lens, retrobulbar fat and bulbar muscles) (Smallwood et al., 2002). The CT anatomy of head cavities has also been described in horses (Solano and Brawer, 2004) and donkeys (El Gendy et al., 2014): few slices were relevant to the orbit, focusing on the relationship with

sinuses, and a limited number of ocular structures were detailed (i.e. eye, lens, periorbital fat and optic nerve). Original studies about MRI anatomy of the eye are scarce and only a few ocular structures were identified in those studies (Morgan et al., 1993; Arencibia et al., 2000).

The objective of this study was to describe CT and MRI anatomy of the equine orbit and ocular globe.

Material and Methods

The heads from two adult ponies and two adult horses, euthanized for reasons unrelated to head and ocular pathology, were used. For acquisitions, both by CT and MRI, the heads were positioned at 45 degrees to the plane of the gantry. This position was used as (1) it is the natural position of the standing horse facilitating understanding of anatomy, (2) it is the position of the head in a horse under dorsal recumbence in general anaesthesia (in that case, dorsal becomes ventral) (Fig. 1).

Computed tomography

Images were acquired by CT with a 6-slice Emotion 6 (Siemens, Erlangen). Acquisition protocol was 130 kV, 80 mAs (pitch 0.4 with tube rotation time of 0.6 s) and collimation 0.63 mm. The images were acquired from 4-cm caudal to the orbit to 5-cm rostral to it. The transverse resolution was 0.44×0.44 mm. Slices of 0.63 mm were reconstructed with an increment of 0.3 mm resulting in an overlap between the different slices and a resultant longitudinal resolution of 0.3 mm without gap. After acquisition, the images were assessed using a medical

digital imaging system (PACS, Telemis, Louvain-La-Neuve, Belgium). Both bony window and soft tissue window were used. Volumes rendered images were also generated to illustrate 3D anatomy of the orbit. Images were viewed in three planes (frontal, transverse and sagittal). The sagittal planes were only used to localize the frontal and transverse planes. Images in transverse planes were viewed from caudal to rostral. The images in frontal planes were examined from dorsal to ventral.

Magnetic resonance imaging

A 3.0 Tesla Siemens Verio 6 was used. T1-weighted (T1W) (0.384×0.360 mm transverse resolution; 3.0 mm slice thickness, 590 ms repetition time; 9.1 ms echo time; distance between slices 3.0 in dorsal planes and 3.6 mm in transverse planes) and T2-weighted (T2W) (0.576×0.522 mm transverse resolution; 3.0 mm slice thickness; 5130.0 ms repetition time for dorsal planes and 5240 ms for transverse planes; 111.0 ms echo time; and distance between slices 3.0 mm) sequences were obtained. An abdominal 6-channel coil was used in combination with a spine coil (Siemens, Germany). Images were transferred on Telemis for analysis. Images were reconstructed in 3D and viewed in three planes (frontal, transverse and sagittal). The sagittal planes were only used to localize the horizontal and vertical planes.

Gross anatomy

To validate CT and MR reference images, these were compared with gross anatomical sections performed with

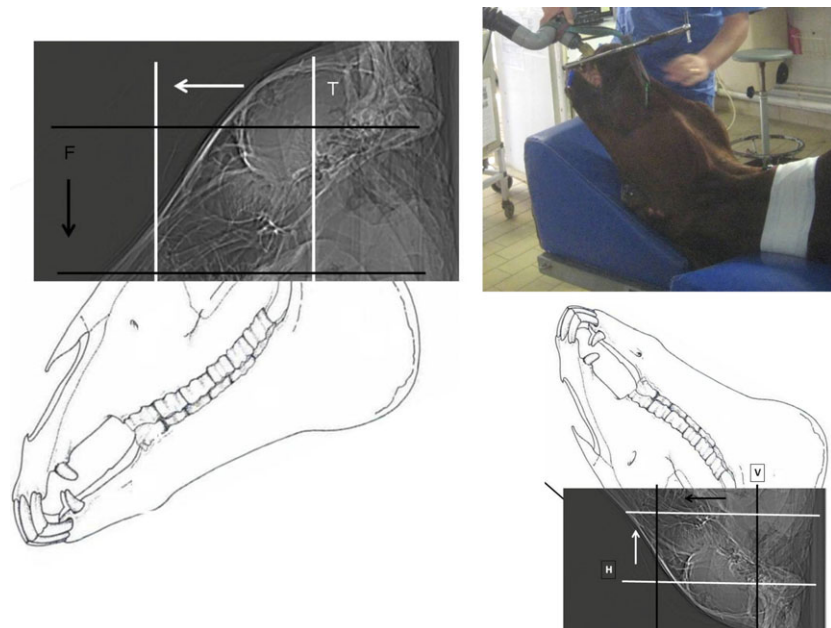


Fig. 1. The head was positioned with its axis at 45° to the plane of the gantry. Vertical planes (white lines), parallel to the gantry, were called transversal (T) while horizontal planes (black lines), perpendicular to the gantry, were called frontal planes (F). Transversal (T) planes were viewed from caudal to rostral (white arrow), while frontal (F) scans were viewed from dorsal to ventral (black arrow).

a thin band saw through the heads after freezing. The sections obtained were 5 mm thick. The gross sections were photographed and compared with MR images for identification of anatomical structures. In addition, to facilitate the identification of the foramina of the skull on CT images, these were compared with an osseous anatomical model that highlighted the foramina and corresponding nerves and vessels (Fig. 2).

Results

Bony limits of orbit

With CT, the orbit could be delineated. It was formed by frontal, zygomatic, temporal, lacrimal, palatine and sphenoid bones. The bony rim completely encircled the globe (Fig. 3). It was shaped by the frontal bone dorsally and its zygomatic process caudally, the zygomatic process of the temporal bone caudoventrally, the temporal process of the zygomatic bone cranioventrally and the lacrimal

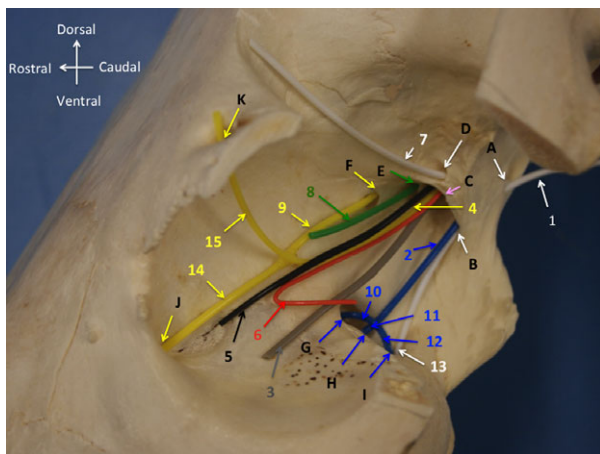


Fig. 2. Anatomical model showing nerves of the orbit and their associated foramina (left lateral view; the zygomatic process of frontal bone, the temporal process of zygomatic bone and the zygomatic process of temporal bone have been transected). A = caudal alar foramen with maxillary artery (white, 1); B = rostral alar foramen with maxillary artery; the rotundum foramen with the maxillary nerve (V-II) (blue, 2) is not visible; C = orbital fissure with the abducens nerve (VI) (grey, 3), the ophthalmic nerve (V-I) (yellow, 4) and the oculomotor nerve (III) (black, 5); the trochlear foramen, with the trochlear nerve (red, 6), close to the orbital fissure, is not visible; D = accessory alar foramen with the rostral deep temporal artery (white, 7); E = optic foramen with the optic nerve (II) (green, 8); F = ethmoidal foramen with the ethmoidal nerve (V-I) (yellow, 9); G = maxillary foramen (leading to the infraorbital canal) with the infraorbital nerve (V-II) (blue, 10); H = sphenopalatine foramen with the sphenopalatine nerve (blue, 11); I = caudal palatine foramen with the palatine nerve (blue, 12) and major palatine artery (white, 13); J = lacrimal foramen with the lacrimal nerve (V-I) (yellow, 14); and K = supraorbital foramen with the frontal nerve (V-I) (yellow, 15).

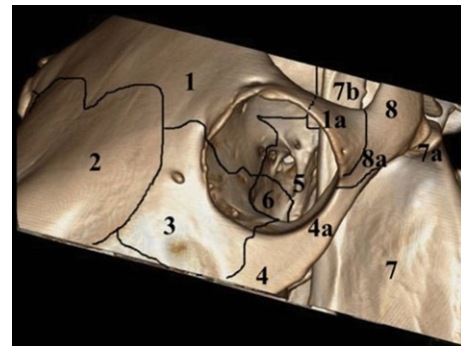


Fig. 3. CT volume rendered image of the orbit. 1. Frontal bone (1a zygomatic process of frontal bone). 2. Nasal bone. 3. Lacrimal bone. 4. Zygomatic bone (4a temporal process of zygomatic bone). 5. Sphenoid bone. 6. Palatine bone. 7. Mandible (7a condylar process of mandible. 7b coronoid process of mandible). 8. Temporal bone (8a zygomatic process of temporal bone).

bone rostrally. The palatine and sphenoid bones constituted the medial wall of the orbital cavity. Caudally, the orbit was not closed by a bony wall but was limited by the coronoid process of the mandible and temporo-mandibular joint.

Foramina

With CT, several foramina could be identified in frontal planes, mostly by proceeding slowly and systematically from dorsal to ventral (Fig. 4). The first to be visualized was the caudal alar (for maxillary artery) foramen

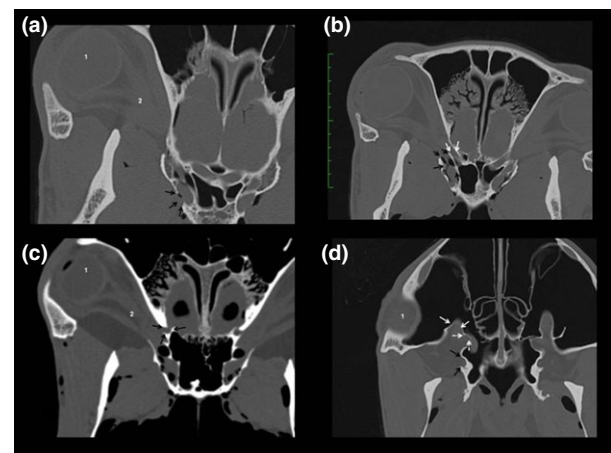


Fig. 4. Frontal CT scans (bony window) from dorsal (a) to ventral (d) showing foramina. 1. Ocular globe. 2. Ocular cone. (a) Arrows indicate the caudal alar foramen. (b) Black arrows show the tract towards the common cranial alar and rotundum foramina joining the orbital fissure. White arrows indicate the optic foramen. (c) Black arrows show the ethmoidal foramen. (d) Maxillary (white arrow), sphenopalatine (white dotted arrow) and palatine (black arrow) foramina.

(Fig. 4a). The tract towards the common cranial alar and rotundum foramina (for maxillary (V-II) nerve) could be identified in a slightly more ventral view, joining the orbital fissure [for abducens (VI), ophthalmic (V-I), oculomotor (III)], while the small trochlear [for trochlear (IV) nerve] and accessory alar foramina could not be distinguished. The optic foramen was identified at the origin of the optical cone (Fig. 4b) and the ethmoidal foramen [for ethmoidal nerve (V-I)] was seen more ventrally and axially (Fig. 4c). Further ventrally and rostrally, the maxillary (for infraorbital nerve, a continuation of the maxillary branch (V-II)), sphenopalatine (for sphenopalatine nerve) and caudal palatine (for palatine nerve and major palatine artery) foramina were identified (Fig. 4d). The lacrimal foramen (lacrimal nerve (V-I)) could be seen in the lacrimal bone on frontal CT scans through the rostral part of the orbit (Fig. 5). The supraorbital foramen (for the frontal nerve) was easily seen on transverse CT images (Fig. 6). Foramina for nerves and vessels could not be identified by MRI.

Relationship with sinuses

Both with CT (Fig. 6) and MRI (Fig. 7), the sinuses and their relationships with the orbit could be identified. They were visible as hypo-attenuated signal in CT planes and as hypo-intense signal in T1W and T2W at MRI. The frontal sinus extended dorsally and ventrally around the orbit and communicated with the caudal maxillary sinus by the frontomaxillary opening, caudally to the medial canthus of the eye. The caudal maxillary sinus was located rostroventrally to the eyeball. The sphenopalatine sinus was seen in the palatine and sphenoid bones ventromedially to the orbit.

Eye and adnexae

The caudoventral orbital cavity was limited by muscles that appeared as an intermediate attenuated signal on CT

soft tissue window scans (Fig. 5) and as an intermediate to hyperintense signal, respectively, on T2W and T1W MRI (Fig. 7). The coronoid process was flanked by the

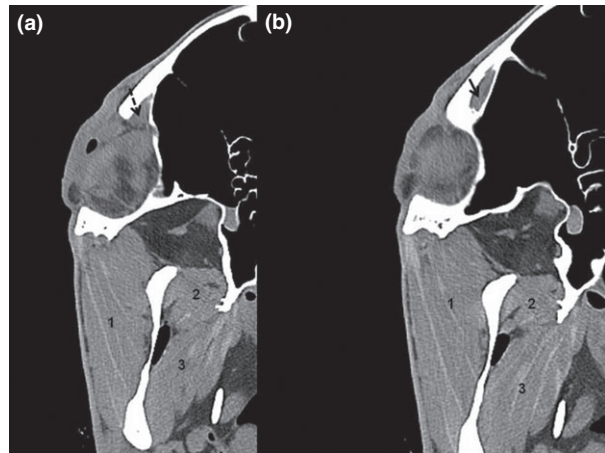


Fig. 5. Frontal CT scan (soft tissue window). 1. M Masseter. 2. M lateral pterygoideus. 3. M medial pterygoideus. Arrows indicate the lacrimal foramen (dotted) and duct (plain).

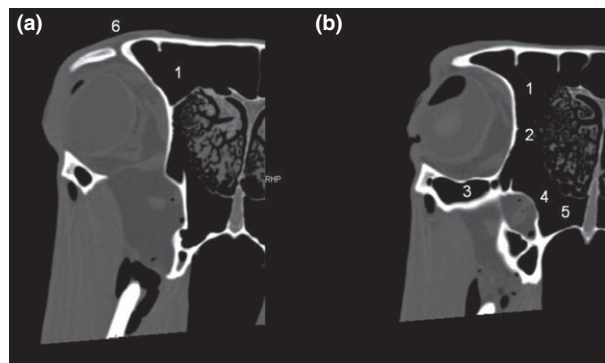
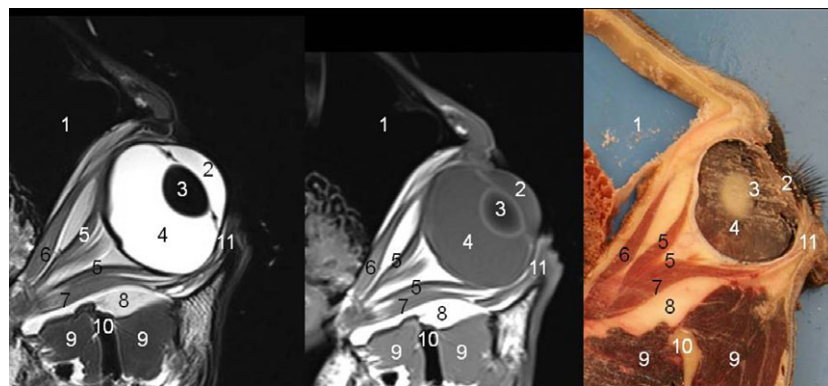


Fig. 6. CT image – bony window (transverse planes) through the caudal part (a) and the rostral part of the orbit (b). 1. Frontal sinus. 2. Frontomaxillary aditus. 3. Caudal maxillary sinus. 4. Aditus towards sphenoplatinus sinus. 5. Sphenopalatine sinus. 6. Supraorbital foramen.

Fig. 7. (Left) T2W image (frontal plane) (Middle) T1W (frontal plane) (Right) Gross anatomical frontal slice. 1. Concho-frontal sinus. 2. Anterior chamber. 3. Lens. 4. Vitreous chamber. 5. M. retractor bulbi. 6. M. rectus medialis. 7. M. rectus lateralis. 8. Periorbital fat. 9. Temporal muscle. 10. Coronoid process. 11. Bony rim.



temporal muscle dorsomedially and dorsolaterally. Rostroventrally to the coronoid process, the lateral and medial pterygoideus muscles flanked the mandible medially and the masseter laterally. Soft tissues were best visualized using MRI.

Fat appeared as a hyperintense signal on T1W and intermediate signal on T2W. It was identified around the orbit and between extraocular muscles (Fig. 7). The periorbita, that is the fibroelastic coat that encircles the extraocular muscles and the optic nerve, was too narrow to be delineated.

The ocular globe was well identified in both planes and both sequences. The vitreous body and chambers appeared white (hyperintense signal) on T2W (Fig. 7), while the lens and the cornea appeared black (hypo-intense signal). The T1W views contrasted the lens (hypo-intense signal) from its capsule (hyperintense signal) (Fig. 7). In a closer T2W view, the ciliary body and the iris could be identified in hypo-intense signal; the frontal plane was the most adequate to view these structures (Fig. 8). It was not possible to distinguish between sclera, choroid and retina.

The lacrimal gland, positioned dorsolaterally to the eyeball and medioventrally to the zygomatic process of the frontal bone, appeared as a lateral oval structure under the upper eyelid (Fig. 9). In T1W, it had an intermediate signal and could be identified close to adjacent periorbital fat (hyperintense signal). In T2W, it had a granular appearance, with an intermediate signal punctuated by some hyperintense particles. The tarsal gland was best visible on transverse T1W views (Fig. 9). It was included in the free edge of the upper eyelid and

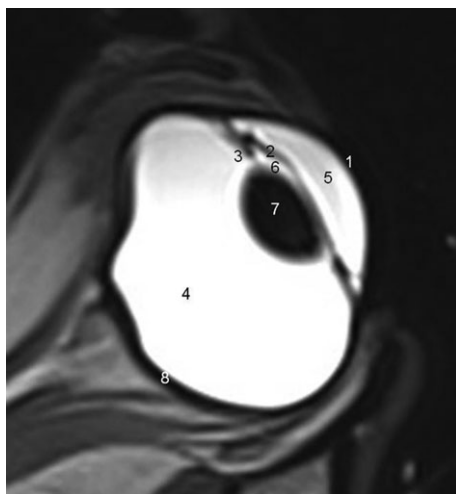


Fig. 8. Frontal T2W. 1. Cornea. 2. Iris. 3. Ciliary body. 4. Vitreous body. 5. Anterior chamber. 6. Posterior chamber. 7. Lens. 8. Retina, choroid, sclera.

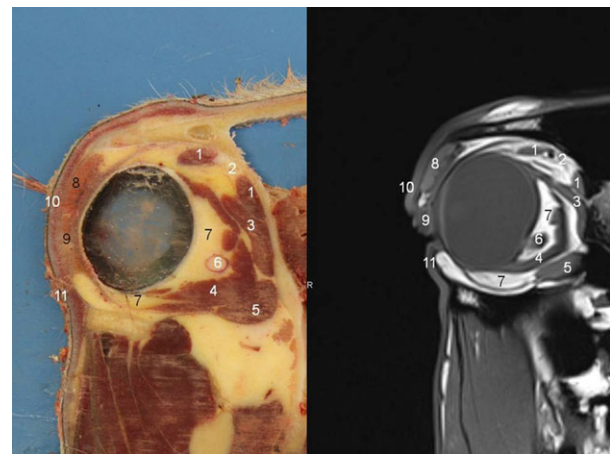


Fig. 9. (Left) Gross anatomical section (transverse). (Right) Transverse T1W. 1. Superior oblique muscle. 2. Trochlea. 3. Rectus dorsalis. 4. Rectus ventralis. 5. Inferior oblique muscle. 6. Optic nerve. 7. Periorbital fat. 8. Lacrimal gland. 9. Tarsal gland. 10. Upper eyelid. 11. Lower eyelid.

appeared slightly more hypo-intense than the lacrimal gland. The third eyelid was identified as an intermediate signal at the medial angle of the eye (Fig. 10).

Muscles were easily identified as an intermediate signal on both T1W and T2W MRI. The rectus muscles (lateralis, medialis, dorsalis and ventralis), superior oblique muscle and levator palpebrae arised from deep in the vicinity of the optic foramen, reaching the globe (for the formers) or the eyelid (for the later). Rectus lateralis and medialis were well identified in frontal views (Fig. 7), while rectus dorsalis and ventralis were best seen in transverse planes (Fig. 9). The superior oblique muscle skated over a trochlea before it inserted on the globe. The trochlea was

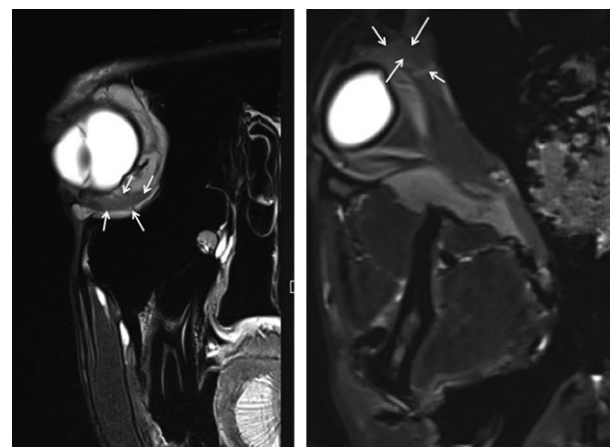


Fig. 10. (Left) Transverse. (Right) Frontal T2W. White arrows indicate the third eyelid.

located dorsomedially. The muscle and the trochlea were both visible on transverse T1W and T2W, although the trochlea was best seen as a hyperintense signal point in T1W (Fig. 9). The inferior oblique muscle originated from a small depression in the medial wall of the orbit, medioventrally to the optic foramen. The insertion of the inferior oblique muscle, arising from the medial wall, could be identified on MRI transverse planes (Fig. 9). The retractor bulbi was found around the optic nerve. It was best visible on frontal T1W and T2W (Fig. 7). The orbicularis and levator palpebrae were poorly delineated both in T1W and T2W.

The path of the nerves could be inferred by the position of their foramina on the CT images (Fig. 4), but were not directly identified by either MRI or CT. The cranial nerve II (optic) was the only nerve that could be seen in section in transverse views (Fig. 9) and longitudinally (reaching the optic chiasma) in frontal views (Fig. 11).

Discussion

The current study demonstrates that CT and MRI are useful techniques to image the equine orbit and eye. Computed tomography identified bony structures, that is the limits of the orbit, its foramina and its relationships with head cavities; however, CT was less useful than MRI in imaging the ocular globe and adnexae. Nerves could not be seen clearly with any technique, except the optic nerve that could be imaged by MRI, while only its tract could be followed by CT. Vessels could not be identified in this series of cadaver heads. Several salient anatomical features were identified.

Bones do not totally limit the orbital cavity and do not totally encircle the globe and its retrobulbar soft tissues. The rostral, dorsal, lateral and ventral limits of the orbit are classically described in textbooks (Budras et al., 2009; Dyce et al., 2010) while the anatomical caudal landmarks

are not commonly highlighted. The current study demonstrated that the caudal limit of the orbit is delineated by a part of the temporal bone, the coronoid process of the mandible, the temporal muscle and the lateral and medial pterygoideus muscles. This absence of bony 'coat' covering the entire orbital cone caudally has clinical implications as this soft tissue compartment could permit access of foreign bodies to the orbit. MRI has previously been used to identify a periorbital wooden foreign body embedded in the masseter muscle, and its precise localization, in a horse with chronic ocular discharge (Santos et al., 2012). Better knowledge of the orbital cavity, its delimitations and its relationships are also important in traumatic injuries where ocular prosthetic devices are considered (Michau and Gilger, 2004).

MRI provided excellent images of soft tissues contained in the orbital cavity. The globe and its different parts (cornea, sclera, lens, iris, ciliary body, vitreous chamber, posterior and anterior chamber) were well detailed in T2W images. T1W images have been reported to provide the best spatial resolution and anatomical details of the eye and orbital structures (Ramirez and Tucker, 2004). In this study, T1W images showed a contrast difference inside the lens, but did not allow the accurate examination of the iris, the ciliary body and of the posterior chamber, in contrast to T2W images. Although a 3.0-Tesla system was used, MRI was not useful for the study of cranial nerves; only the optic nerve (II) was clearly seen, from its exit of the globe to the optic chiasma. One other limitation of the current study was the use of cadavers impeding the study of blood vessels.

Ultrasonography (US) is commonly used in ophthalmology (Penninck et al., 2001). Although the current study was not designed to compare CT and MRI with US, it is worth discussing the potential applications of the different imaging modalities. Ultrasonography has been reported to be able to identify lesions of the anterior segment of the ocular globe associated with trauma such as lens luxation, hyphema and inflammatory material in the anterior chamber (Williams and Wilkie, 1996). Intraocular masses (inflammatory, neoplastic and cystic) can be assessed by US; as many lesions arise from the anterior uvea, they can be difficult to diagnose without an offset device, extra coupling gel or scanning through closed eyelids (Williams and Wilkie, 1996). In addition, the posterior chamber is not always seen ultrasonographically in normal equine eyes because of its small dimensions (Rogers et al., 1986). MRI consistently identified the anterior and posterior chambers in the four heads in the current study. US can also be used to evaluate the posterior segment for abnormalities of the vitreous and the retina (Williams and Wilkie, 1996). The retina cannot be clearly delineated from the underlying choroid and sclera (Reef,

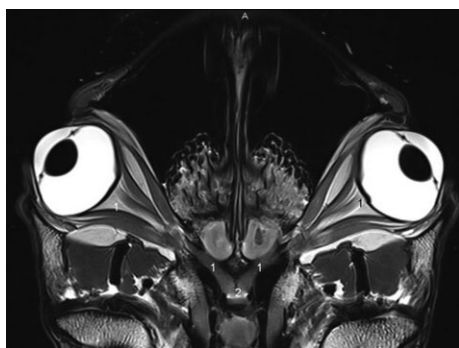


Fig. 11. Frontal T2W. 1. Optic nerve. 2. Optic chiasma.

1998; Wilke and Gilger, 1998). This was also the case with MRI in this study. One advantage of US is that echoes may demonstrate motion (Williams and Wilkie, 1996) such as in vitreous haemorrhage and retinal detachment. This is not possible with MRI. One disadvantage of US is that structures beyond bony surfaces are not imaged (Wilke and Gilger, 1998). It is difficult to assess the extent and severity of bony involvement using this technique. Therefore, in bony invasion/lysis, CT or MRI is recommended to assess fully the extent of the pathological process (Davis et al., 2002), for example for assessment of muscles in human medicine. US provides limited information about bony and periocular tissues (Williams and Wilkie, 1996; Penninck et al., 2001; Bentley et al., 2003). MRI identified well adnexae in the current study. Nevertheless, US is a rapid, safe and practical method. On the other hand, CT and MRI suffer from technical difficulties, including the need for general anaesthesia and limited availability.

In the future, it is likely that high field MRI systems will become more and more available and will have several applications in equine ophthalmology. More studies on diseased eyes and orbits are warranted to determine the value of those imaging tools in equine ophthalmology.

Acknowledgements

We acknowledge V. Simon, R. Graffin, Y. De Raeve, for their help. We thank the team of Mont Godinne Hospital: R. Vanderstricht and M. Tallier, for their contribution. We are grateful to Siemens Belgium, Guerbet Belgium and La Fondation Mont Godinne for their support.

Role of the Funding Source

This study was supported by the University of Namur (UNamur), NARILIS (Namur Research Institute for Life Science) and The Fondation Mont Godinne (CHU-Dinant Mont Godinne).

Competing Interests

None of the authors of this paper has a financial or personal relationship with people or organizations that could inappropriately influence or bias the content of the paper.

References

Arencibia, A., J. M. Vázquez, R. Jaber, F. Gil, J. A. Ramirez, M. Rivero, N. Gonzales, and E. R. Wisner, 2000: Magnetic resonance imaging and cross sectional anatomy of the

normal equine sinuses and nasal passages. *Vet. Radiol. Ultrasound* **41**, 313–319.

- Bentley, E., P. E. Miller, and K. A. Diehl, 2003: Use of high-resolution ultrasound as a diagnostic tool in veterinary ophthalmology. *J. Am. Vet. Med. Assoc.* **223**, 1617–1622.
- Budras, K. D., W. O. Sack, and S. Rock, 2009: *Anatomy of the Horse—An Illustrated Text*, 5rd edn. Hannover: Schlutersche, pp. 38–49.
- Caha, C. M., S. E. Kirschner, K. E. Baer, and J. D. Stefanacci, 1994: The use of computed tomography scans for the evaluation of orbital disease in cats and dogs. *Vet. Comp. Ophthalmol.* **4**, 24–30.
- Davis, J. L., B. C. Gilger, K. Spaulding, I. D. Robertson, and S. L. Jones, 2002: Nasal adenocarcinoma with diffuse metastases involving the orbit, cerebrum, and multiple cranial nerves in a horse. *J. Am. Vet. Med. Assoc.* **221**, 1460–1463.
- Dennis, R., 2000: Use of magnetic resonance imaging for the investigation of orbital disease in small animals. *J. Small Anim. Pract.* **41**, 145–155.
- Dyce, K. M., W. O. Sack, and C. J. G. Wensing, 2010: *Textbook of Veterinary Anatomy*, 4rd edn. Missouri: Saunders Elsevier, pp. 57–67, and pp. 315–334.
- El Gendy, S. A. A., M. A. M. Alsafy, and A. A. El Sharaby, 2014: Computed tomography and sectional anatomy of the head cavities in donkey (*Equus asinus*). *Anat. Sci. Int.* **89**, 140–150.
- Michau, T. M., and B. C. Gilger, 2004: Cosmetic globe surgery in the horse. *Vet. Clin. North Am. Equine Pract.* **20**, 467–484.
- Morgan, R. V., G. B. Daniel, and G. B. Donnell, 1993: Magnetic resonance imaging of the normal eye and orbit of the horse. *Prog. Vet. Comp. Ophthalmol.* **3**, 127–133.
- Morrow, K. L., R. D. Park, T. L. Spurgeon, T. S. Stashak, and B. Arceneaux, 2000: Computed tomographic imaging of the equine head. *Vet. Radiol. Ultrasound* **41**, 491–497.
- Penninck, D., G. B. Daniel, R. Brawer, and A. S. Tidwell, 2001: Cross-sectional imaging techniques in veterinary ophthalmology. *Clin. Tech. Small Anim. Pract.* **16**, 22–39.
- Ramirez, S., and R. L. Tucker, 2004: Ophthalmic imaging. *Vet. Clin. North Am. Equine Pract.* **20**, 441–457.
- Reef, V. B., 1998: Ultrasonographic evaluation of small parts. In: *Equine diagnostic ultrasound*. (V. B. Reef, ed). Philadelphia: WB Saunders. pp. 480–547.
- Rogers, M., R. E. Cartee, W. Miller, and A. K. Ibrahim, 1986: Evaluation of the extirpated equine eye using B-mode ultrasonography. *Vet. Radiol.* **27**, 24–29.
- Santos, M., S. D. Gutierrez-Nibeyro, A. A. Stewart, R. Hyde, and D. Rodgerson, 2012: Identification of a periorbital wooden foreign body as the cause of chronic ocular discharge in a horse. *Aust. Vet. J.* **90**, 84–87.
- Schaer, B. D., 2007: Ophthalmic emergencies in horses. *Vet. Clin. North Am. Equine Pract.* **23**, 49–65.

- Smallwood, J. E., B. C. Wood, W. E. Taylor, and L. P. Tate, 2002: Anatomic reference for computed tomography of the head of the foal. *Vet. Radiol. Ultrasound* **43**, 99–117.
- Solano, M., and R. S. Brawer, 2004: CT of the equine head: technical considerations, anatomical guide, and selected diseases. *Clin. Tech. Equine Pract.* **3**, 374–388.
- Wilke, D. A., and B. C. Gilger, 1998: Equine diagnostic ocular ultrasonography. In: *Equine diagnostic ultrasonography*. (N. W. Rantanen and A. O. McKinnon, eds). Baltimore: Williams & Wilkins. pp. 637–645.
- Williams, J., and D. Wilkie, 1996: Ultrasonography of the eye. *Compend. Contin. Educ. Pract. Vet.* **18**, 667–677.